Network structure governs Drosophila brain functionality

Xiaoyu Zhang [a,b,c], Pengcheng Yang [a], Jiawei Feng [a], Kang Wen [a], Gang Yan [d], Qiang Luo [c], Wei Lin [c], Xin Lu [a,*]

[a] College of Systems Engineering, National University of Defense Technology, Changsha 410073, China
[b] Xiangjiang Laboratory, Changsha 410205, China
[c] Research Institute of Intelligent Complex Systems, Fudan University, Shanghai 200433, China
[d] MOE Key Laboratory of Advanced Micro-Structured Materials, and School of Physical Science and Engineering, Tongji University, Shanghai 200092, China

ABSTRACT

How intelligence emerges in living beings is a fundamental but largely unanswered question in neuroscience. To address this challenge, we leveraged the largest available data set of adult Drosophila connectome, and constructed a comprehensive computational framework using simplified neuronal activation mechanisms to mimic the observed activation behavior within the connectome. The results revealed that even with rudimentary neuronal activation mechanisms, models grounded in real neuronal network structures can generate activation patterns strikingly analogous to those observed in the actual brain. A significant discovery was the consistency of activation patterns across various neuronal dynamic models with the same network structure. This consistency results therefore underscore the pivotal role of network topology in neural information processing, but challenge the prevailing view that solely relies on neuron count or complex individual neuron dynamics. Further analysis demonstrated a near-complete separation of the visual and the olfactory systems at the network level. Moreover, we found that the network distance, rather than spatial distance, is the primary determinant of activation patterns, and also that a reconnect rate of at least $1^o/_{oo}$ was sufficient to disrupt the previously observed activation patterns. We also observed synergistic effects between the brain hemispheres: Even with unilateral input stimuli, visual-related neurons in both hemispheres were activated, highlighting the importance of interhemispheric communication. All these findings suggest the crucial role of network structure in neural activation and offer novel insights into the fundamental principles governing brain functionality.

1. Introduction

The neural systems of intelligent beings maintain continuously dynamical communication [1]. This process gives rise to macroscopic emergence across the entire neural system. Such communication fosters the emergence of intelligence in all intelligent life forms. Consequently, comprehending and replicating this process has become an indispensable avenue for unraveling biological intelligence and realizing artificial intelligence [2].

Neural systems are often modeled as interconnected networks [3], with neurons engaging in constant communication via synapses within the network's topology. To elucidate the relationship between the network itself and its dynamics in a neural network, various models have been developed, spanning from the cellular level to the whole brain. For example, neuronal dynamic models like Leaky Integrate-and-Fire (LIF) model [4] are designed to describe the electrical activity and dynamic behavior of neurons [5,6]. These models are characterized by the following features: they typically use a set of differential equations to describe the electrophysiological behavior of neurons and usually contain a set of parameters that need to be measured experimentally or estimated. On a larger scale, a vast array of isolated neuronal dynamics, ranging from several to millions, are interconnected and parameter-optimized to simulate the local or global dynamics of the brain [7]. The implementation of these high-fidelity neuronal models necessitates extraordinary levels of data precision and imposes substantial computational demands that often exceed the capabilities of current technological infrastructure. This approach prompts a critical inquiry into whether a complete, one-to-one replication of neuronal dynamics is an absolute prerequisite for accurately modeling brain behavior and cognitive functions. Another category of network-based methods applies propagation models on complex networks to neural networks, thereby describing information propagation and emergent mechanisms within neural networks. These methods are collectively referred to as brain network communication models. Such approaches typically involve substantial simplification of neuron

* Corresponding author.
E-mail addresses: xyzhangphd@outlook.com (X. Zhang), yangpengcheng@nudt.edu.cn (P. Yang), fengjiawei126@gmail.com (J. Feng), wenkang@nudt.edu.cn (K. Wen), gyan@tongji.edu.cn (G. Yan), qluo@fudan.edu.cn (Q. Luo), wlin@fudan.edu.cn (W. Lin), xin.lu.lab@outlook.com (X. Lu).

models, resulting in fewer parameters, but also leading to the loss of some electrophysiological details of neurons [8]. These two seemingly opposing approaches illustrate that it remains unresolved whether the neuronal dynamics or the connectivity between neurons play the more dominant role. This question is fundamental to understanding how intelligence emerges from neural systems.

Additionally, in recent years, as an innovative way to modify intelligence, artificial neural networks (ANNs) have achieved significant advancements in numerous fields [9,10]. Despite these achievements, the structure of ANNs does not strictly mimic the actual neural network structure of biological brains. This discrepancy raises questions about the hypothesis that the inherent structure of a network is crucial for intelligence. Furthermore, the scaling law in the field of machine learning posits that the more parameters an ANN has, the greater the degree of emergent intelligence it can exhibit [11]. These theory hints that the quantity of neurons (parameters) might be a more significant factor in the development of intelligence than the precise arrangement of these neurons in a network, suggesting that the specific network structures found in biological systems may not be essential for the emergence of intelligence.

The observation of neural network structures is crucial for interpreting intelligence from a network perspective. Current neuroimaging techniques, such as Magnetic Resonance Imaging (MRI) and functional MRI (fMRI), offer non-invasive exploration but lack the spatial resolution necessary to resolve individual neurons and synapses. However, these measurement methods face challenges in obtaining information about the positions and connectivity of neurons in the nervous system, making it difficult to understand the nervous system at the neuron-synapse level [12]. Employing electron microscopy (EM) and deep learning techniques for automated neuron reconstruction, brain atlases of a range of animals, including Drosophila larvae [13], have been mapped. A recent study [14] published an adult Drosophila connectome data set, comprising nearly 130,000 neurons and 50,000,000 synapses, with details of neuronal network structure at unforeseen resolution. With full proofreading of the central brain and approximately 80% completion of the optic lobesis presented, the data represents the largest whole-brain connectome of an adult Drosophila to date and provides an unprecedented opportunity for comprehensive network analysis and topological characterization of the Drosophila brain.

Building on the outlined challenges and opportunities, this study utilized the aforementioned Drosophila connectome data set [14] to examine the importance of neuronal network's structure in simulating brain activation patterns. We constructed a large-scale network communication model framework based on simple mechanisms to simulate activation behavior observed in the connectome. Initially, we established a network representation of the connectome. We then developed a large-scale network communication model where neurons activate upon receiving sufficient stimuli and transmit signals to other neurons. This iterative process generated a global activation pattern. Our analysis employed threshold and sigmoid models as baselines, with a LIF model for comparison. We proposed an evaluation criterion based on the ratio of actual to expected neuron activations.

Additionally, we developed a 3D network visualization tool (for details, pelase refer to supplementary materials), using HTML5's Canvas and Three.js based on WebGL technology. This software enables real-time observation of each neuron's communication process in three dimensional space.

2. Data and methods

2.1. Drosophila connectome data set

We utilize the recently released largest Drosophila brain connectome [14], which provides a comprehensive mapping of the entire neural network within a female Drosophila brain. This data set includes over 120,000 neurons and 50,000,000 synapses, featuring detailed synaptic connections and high-precision 3D coordinates (accurate to the nanometer level) for both cell bodies and synapses. Additionally, it offers extensive labeling for various neuron types. Fig. 1 is a visualization of the Drosophila connectome. Visually, the shape of most of the functional regions of the brain appears to be physically similar. For more detailed information, refer to [14,15].

In this section, neurons are represented as nodes and synapses as connections between them. Table 1 presents the basic properties of the data set. We combine multiple edges between two nodes to calculate network statistics. The average degree before and after combining multiple edges is 501.6 and 37.01, respectively, indicating the prevalence of multiple synapses between pairs of neurons.

2.2. Large scale network communication model with neuronal dynamics

In this section, we introduce the large scale network communication model (LSNC) which consumes less computational resource and can efficiently utilize the network structure. To solve the problem that the link weights between neurons can't be measured, we propose two hypotheses to estimate the link weights. In addition, we replace the node model in the network communication model with an improved LIF neuron model for comparison.

2.2.1. Symbol systems

The original network dynamic model of neural systems often uses nodes to represent neurons and edges to represent the links (chemical synapses, electrical synapses, etc.) between neurons [3]. However, multiple synapses typically exist between two neurons [16] For instance, two neurons can have multiple synapses with varying dynamic properties. Simultaneously, due to data limitations, it is challenging to apply conventional methods to describe the dynamics on networks with complex interconnections. For this reason, we use the dual method [17] on Drosophila connectome data set to establish the neuronal network communication model.

In a dual graph, the nodes and edges of the original graph are interchanged, resulting in a new graph. In simple terms, a dual graph is obtained by replacing the nodes of the original graph with edges, and the edges with nodes. After being processed, the nodes in the dualed graph represent the synapses and links represent the cell body. Then we can use the communication model to describe the message propagation process.

In order to standardize the symbol system, we use a edge (multi-edge, could include more than 2 nodes) to represent the neuronal cell body and use an node to represent a physical link between neurons (synapse). We regard the process of messages interactions as the nodes' interactions via edges.

Let $N = \{n_1, \ldots, n_i, \ldots\}$ represents the set of all nodes and $E = \{e_1, \ldots, e_j \ldots\}$ represents the sets of all edges. An obvious relationship is formalized as the following manner.

$$e_k \cap e_q = \{n_i | (n_i \in e_k) \wedge (n_i \in e_q)\}. \tag{1}$$

Note that the union of each element in N and E is the whole graph. The graph G's definition is given as follows.

$$G = \bigcup_j e_j = \bigcup_i \{n_i\}. \tag{2}$$

Let the label of any neuron be j. Because neural link is directed, let e_j^+ (e_j^-) represent the set of elements which output (input) the signals, note that $e_j = e_j^+ \cup e_j^-$.

Each neuron and synapse has an activate state (state = 1) or resting state (state = 0). When a neuron is at the activate state, it fires to other neurons, otherwise it keeps rest. So set the statement of the element i as X_i. $X_i = 1$ if the element n_i is active, otherwise $X_i = 0$. Then let Y_j represent the statement of set e_j. $Y_j = 1$ if the set e_j is active, otherwise $Y_j = 0$.
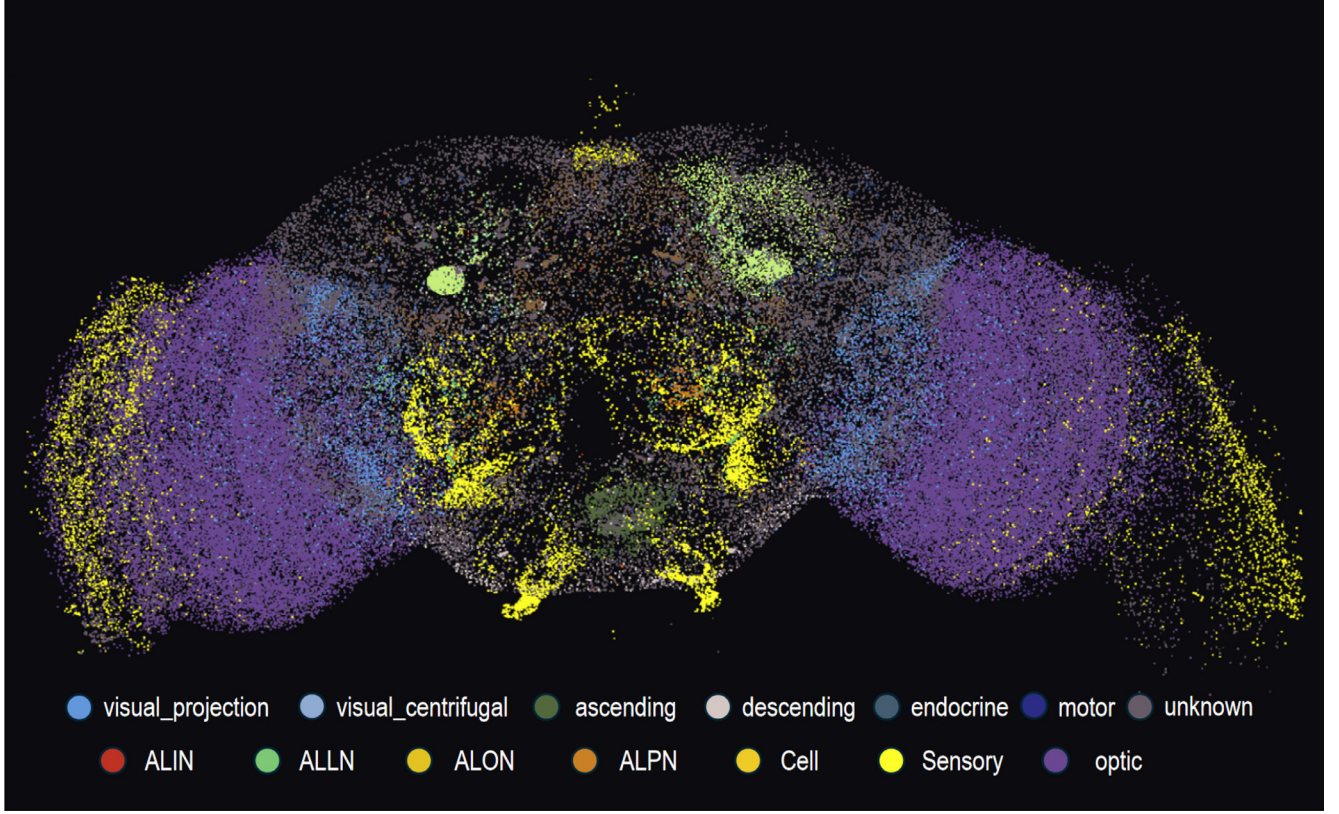
Fig. 1. Visualization of Drosophila connectome. The different colors represent different functional regions.

Table 1

Statistical Properties of Drosophila Brain Connectome Graph.

Property	Description	Value
Number of Nodes	Total number of neurons	131,459
Number of Edges	Total number of synaptic connections	32,970,606
Average Degree	Average number of connections per neuron	37.01
Average Degree (before combination)	Degree before merging connections	501.6
Clustering Coefficient	Measure of local connectivity	0.1527
Eigenvector Centrality	Influence of a neuron in the network	0.0008817
Network Diameter	Longest shortest path in the network	11
Average Shortest Path	Mean shortest path length	3.9061
Assortativity Coefficient	Tendency of nodes to connect to similar nodes	−0.05868

2.2.2. Large scale network communication model (LSNC)

By modeling the Drosophila connectome as graph, we introduce the large scale network communication model on this graph. The general transmission function is defined in the following manner,

$$Y_j = \sigma\left(\frac{1}{\beta_j} \sum_{i|e_i^+ \cap e_j^- \neq \emptyset} \sum_{k|n_k \in e_i^+ \cap e_j^-} \omega(n_k, e_i, e_j) X_k\right), \quad (3)$$

where $\omega(n_k, e_i, e_j)$ represents the link weight between set i and set j (specifically, two neurons) through element n_k. Here we consider that the link weight between two neurons is not only related to the neurons themselves, but also to the synapses between them. $\sigma(.)$ is the activate function. β_j is the normalization factor.

In this paper we use threshold activation function and sigmoid function for comparison. The threshold activation function is a simple, binary decision function used in artificial neurons. It outputs a value of 1 if the input exceeds a certain threshold, and 0 otherwise. This function is also known as the Heaviside step function.

$$\sigma(x) = \begin{cases} 1 & x \geq threshold \\ 0 & x < threshold \end{cases} \quad (4)$$

The sigmoid activation function is a smooth, S-shaped function that maps input values to an output range between 0 and 1. It is commonly used in neural networks to introduce non-linearity and to model probability-like outputs in binary classification problems. The sigmoid function is defined as the logistic function.

$$\sigma(x) = \frac{1}{1 + e^{-x}} \quad (5)$$

The state of an neuron will influence the state of all output synapses. The equation between neuron j and output synapse i is as the following manner.

$$X_i = Y_j \quad if \ n_i \in e_j^+. \quad (6)$$

In neural network models, synaptic link weights are typically employed to characterize the strength of interactions between neurons. Larger link weights mean a tighter "link" between two neurons. However, existing experimental methods are not well-suited for directly measuring the weights between neurons in a whole brain, so adopting some alternative approach is necessary. Below, we introduce a hypothesis that use different methods to estimate the connection weights between neurons: We assume that the source neuron has the same influence on the

target neuron through every synapse, which is widely used in neuron graph statistics analysis [18]. That is to say,

$$\omega(n_k, e_i, e_j) = 1. \tag{7}$$

Additionally, We denote the sum of all link weights between neurons i and j as W_{ij}:

$$W_{ij} = \sum_{k|n_k \in e_i^+ \cap e_j^-} \omega(n_k, e_i, e_j). \tag{8}$$

And we define β_j as the maximum weight among all W_{ij} related to neuron j. That is to say,

$$\beta_j = Max(\{W_{ij} | e_i^+ \cap e_j^- \neq \emptyset\}). \tag{9}$$

Where $Max(S)$ represents the maximal element in set S.

Then the normalized equation is as follows.

$$Y_j = \sigma\left(\frac{1}{\beta_j} \sum_{i|e_i^+ \cap e_j^- \neq \emptyset} \sum_{k|n_k \in e_i^+ \cap e_j^-} \omega(n_k, e_i, e_j) X_k\right). \tag{10}$$

2.2.3. Neuron dynamic model

To better reflect real-world conditions and demonstrate that the superiority of this network architecture does not solely rely on the design of the activation function, we also employed a variant of the LIF model [4] as the basic neuron model.

The membrane potential change of a neuron's voltage can be described by the following differential equation:

$$V_j(t + dt) = V_j(t) + \left(\frac{dt}{\tau}\right) \times \left(R \cdot I_j^{syn} - (V_j(t) - V_{\text{reset}})\right). \tag{11}$$

Where V_j represents the membrane potential of jth neuron, R represents the resistance constant and I_j^{syn} represents the total input current of neuron j. τ represents the time constant.

The current I_j^{syn} can't be observed directly. To estimate the value of I^{syn}, we make the following assumptions based on the following supposes:

1. The magnitude of the current on the synapse should be proportional to the voltage difference between the connected neurons.

2. The current on each synapse should be proportional to the connection weight between the neurons.

3. A current can only be emitted if the output neuron is in an active state.

Considering the supposes above, the equation of input current I_j^{syn} is designed as follows:

$$I_j^{\text{syn}} = \frac{1}{\alpha \beta_j} \sum_{i|e_i^+ \cap e_j^- \neq \emptyset} \sum_{k|n_k \in e_i^+ \cap e_j^-} \left(\omega(n_k, e_i, e_j)\right) \times (V_i - V_j) \times Y_i\right) \tag{12}$$

where $V_i - V_j$ represents the voltage difference between neuron i and j. Y_i represents the state of output neuron i. β_j is defined according to Eq. (9). α is the proportion const.

According to the LIF model, when a neuron's voltage reaches the threshold value, the neuron will fire and then quickly resets its voltage. Based on this, the mechanism for updating the neuron voltage is designed as follows.

$$\begin{array}{ll} \text{if } V_j \geq V_{th} & : \ Y_j = 1 \text{ and } V_j = V_{\text{rest}} \\ \text{else} & : \ Y_j = 0 \end{array}, \tag{13}$$

where V_{th} represents the fire voltage and V_{rest} represents the rest voltage, respectively.

2.3. Evaluation criteria

In previous study, researchers used classic indicators such as signaling cost and activation time to evaluate the quality of the model [8,19,20]. However, these indicators can't describe the model accords with the true communication process or not, even if the activation time is short and the signaling cost is minimum, etc. To better assess whether a model can reflect the real situation of brain communication, we use the percentage of activated neurons in regions that related to (should work under) a certain stimulus. To illustrate, if the brain gets a visual stimulus, the region related to vision should work while the region not related to vision should remain a resting state. Then we record the percentage of neurons activated. If regions related to the certain function have a significant higher activation percentage than the average activation percentage of the whole brain, we call it a quasi-real activation pattern.

We define the consistency indicator C in a area which has a certain function (vision, olfaction, etc) is defined in the following manner.

$$C = N^{act}/N, \tag{14}$$

where N^{act} represents the number of neurons activated in this area at the final state, N represent the number of neurons in this area and N represent the total number of neurons.

2.4. Experimental settings

The basic methodology of the experiment is as follows. We apply a continuous stimulus signal (binary 0–1 signal) to a subset of input neurons (i.e., visual or olfactory neurons) in the brain. We then compute the signal's propagation process within the brain and record the responses of both intermediate and output neurons. We give 2 types of input neurons (visual, olfactory) stimulus and record the activation patterns of 6 type of neurons: optic (visual), visual_projection (visual), ALLN (olfactory), ALIN (olfactory), ALPN (olfactory) and ALON (olfactory). When we give neuron a stimulus, we set the state of neuron as 1. The evaluation criterion involves calculating the ratio of neurons that should be activated to those that are actually activated in a specific area (see Eq. 14).

Given that the brain functions similarly to a shallow neural network [21], we document outcomes at an iteration step size of 5. Since the input is constant and no randomization parameters are introduced, the results of each experiment are consistent, eliminating the need for repetition. For detailed information on related neurons, please read Section "Introduction of Related Neurons" in supplementary materials.

In the linear threshold model, we set $\sigma_0 = 0.8$. For the simulation of the LIF model, numerous hyperparameters are required. All the hyperparameters used are listed in the following table. Biological hyperparameters are set according to real biological experimental tests [22]. The current proportion factor is the optimal parameter obtained through equidistant search.

To demonstrate the importance of network structure, we add a comparative model that randomly reconnects networks. Specifically, we perform degree-preserving rewiring on a certain proportion of edges in the brain, which means perturbing the network structure while ensuring that the degree of each node remains unchanged. In Fig. 3 we set reconnect rate $p = 20\%$. For its sensitivity analysis, please read Section 3.6.

3. Experimental results

3.1. Structural properties of drosophila connectome

From Fig. 2(a) we can see that the degree, i.e., the number of connections to the nodes in the network, exhibits a long-tail distribution, implying that while a large number of neurons possess few synapses, a small number of neurons contains a large number of synapses. For example, more than 20% of the nodes have a degree greater than 50, while only 0.3% of the nodes have a degree greater than 500. This is consistent with previous research on functional brain networks [23].

To investigate whether the two hemispheres' network structures are similar in network statistic properties, we conducted a comprehensive network analysis on the two hemispheres. We calculated the degree,
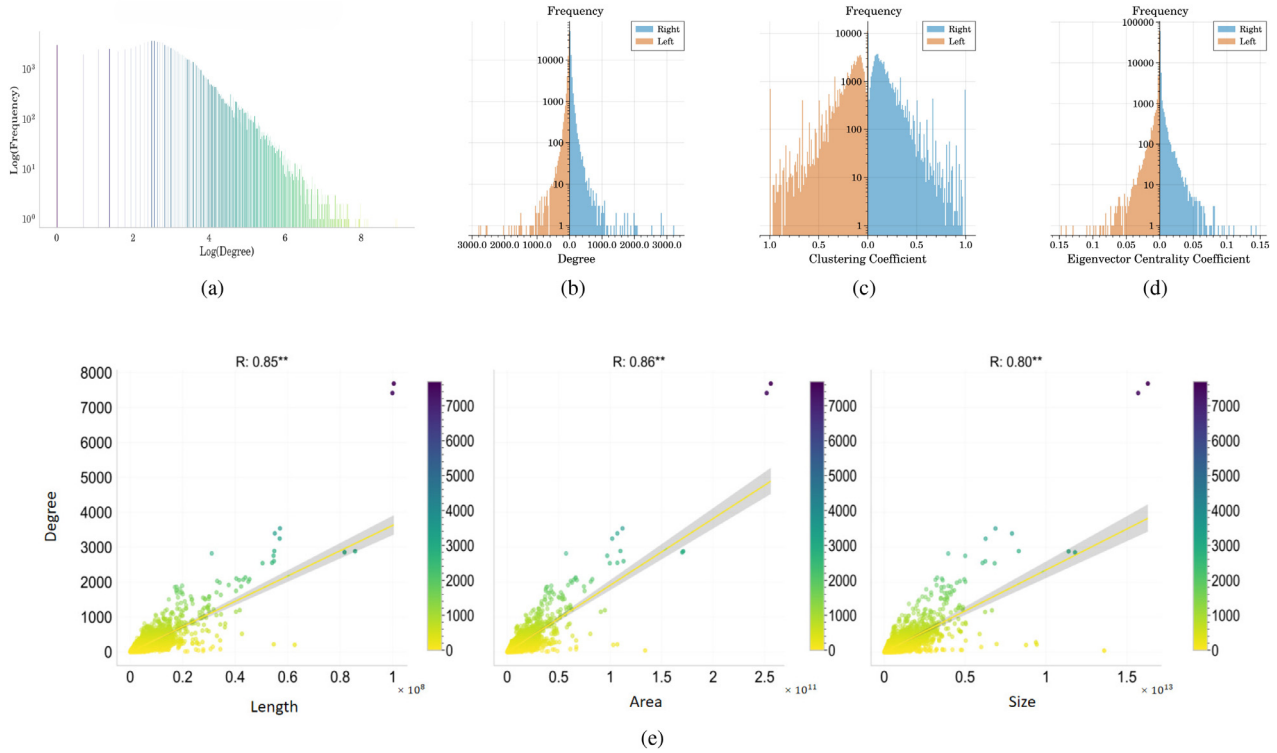
(a)   (b)   (c)   (d)

(e)

Fig. 2. Statistic properties of Drosophila connectome data set. (a) shows the degree distribution of the network. (b), (c) and (d) plot the distribution of degree, clustering coefficient, and eigenvector centrality in each hemisphere, respectively. (e) represents the correlation between degree distribution and neuron characteristics. We use nodes to represent neurons' cell bodies and use edges to represent the synapses when calculated statistic properties.

clustering coefficient, and eigenvector centrality distribution for every node in each hemisphere. According to Fig. 2(b)-(d), these statistical indicators for both hemispheres are extremely similar, indicating that the brain exhibits strong symmetry in network structure.

Also, we plotted the correlation curves between degree and cell length, cell surface area, and cell size (Fig. 2(e)). The significance coefficients R are 0.85 ($p = 0.00$), 0.86 ($p = 0.00$), 0.80 ($p = 0.00$), respectively. The results indicate that the degree is logarithmically linearly correlated with these characteristics. This logarithmic relationship reveals a fundamental principle in the organization of neural networks in the brain.

3.2. Activation patterns under different type of stimuli

In this section, we investigate the impact of different activation mechanisms on network activation patterns by utilizing various network activation mechanisms and observing the changes in activation rates across different areas of the network. Simultaneously, we examine the effect of global perturbations in network structure on activation patterns by altering the network architecture. The optic and visual_projection area are related to vision. ALLN, ALIN, ALON and ALPN are related to olfaction. Other supplemental messages of related neurons are presented in Section "Introduction of Related Neurons" in supplementary materials.

Fig. 3 illustrates the activation patterns of the large-scale network communication model (LSNC) using threshold, sigmoid, and LIF activation mechanisms. We also evaluated the model's performance after introducing perturbations. For a detailed description of these models, please refer to "Data and Methods".

From left subgraphs of Fig. 3 (a) and (b), it can be observed that the network model generates quasi-real activation patterns under specific stimuli: It is evident that visual (olfactory) stimuli result the most significant activation on visual (olfactory) neurons such as optic and visual

projection neurons (ALLN, ALIN, ALPN, ALON neurons) while activating other neuron types minimally.

Our findings indicate that different activation mechanisms can yield comparable activation patterns. In response to visual stimuli, all three models displayed notable activation in visual-related areas, whereas other areas exhibited minimal activation (left subgraphs of Fig. 3 (a), (c), and (e)). The optic area, for instance, recorded activation rates of 36.39%, 4.69%, and 9.69%. Under olfactory stimuli, the network also exhibits similar activation patterns in olfactory-related areas, with average activation rates of 94.07%, 78.01%, and 69.75%, respectively (left subgraphs of Fig. 3 (b), (d) and (f)). This suggests that the connectivity between neurons is more critical than the activation mechanisms of individual neurons.

However, in the perturbed models (right subgraphs of Fig. 3(a)–(f)), the original quasi-real activation patterns disappear. No significant differences in activation regions were observed across all activation modes and types of stimuli. For instance, in the model with threshold activation mechanism, the maximum difference of all areas in the activation ratios under visual stimuli was only 3.162%, and the range of regional activation ratios versus the average activation ratio was only 6.32% (right subgraph of Fig. 3(a)), which indicates that the heterogeneity between different regions completely disappears. Additionally, in the sigmoid and LIF models, no significant activation was observed in any area.

Despite variations in activation rates among the three models, the substantial disparity between the activation ratios of relevant and irrelevant areas suggests the emergence of comparable quasi-real activation patterns across all models.

3.3. Separation of visual and olfactory related areas

To further investigate the causes of the above observed dynamic pattern that is independent of neuron models, we calculated the synapse count (number of connections) between various regions of the visual
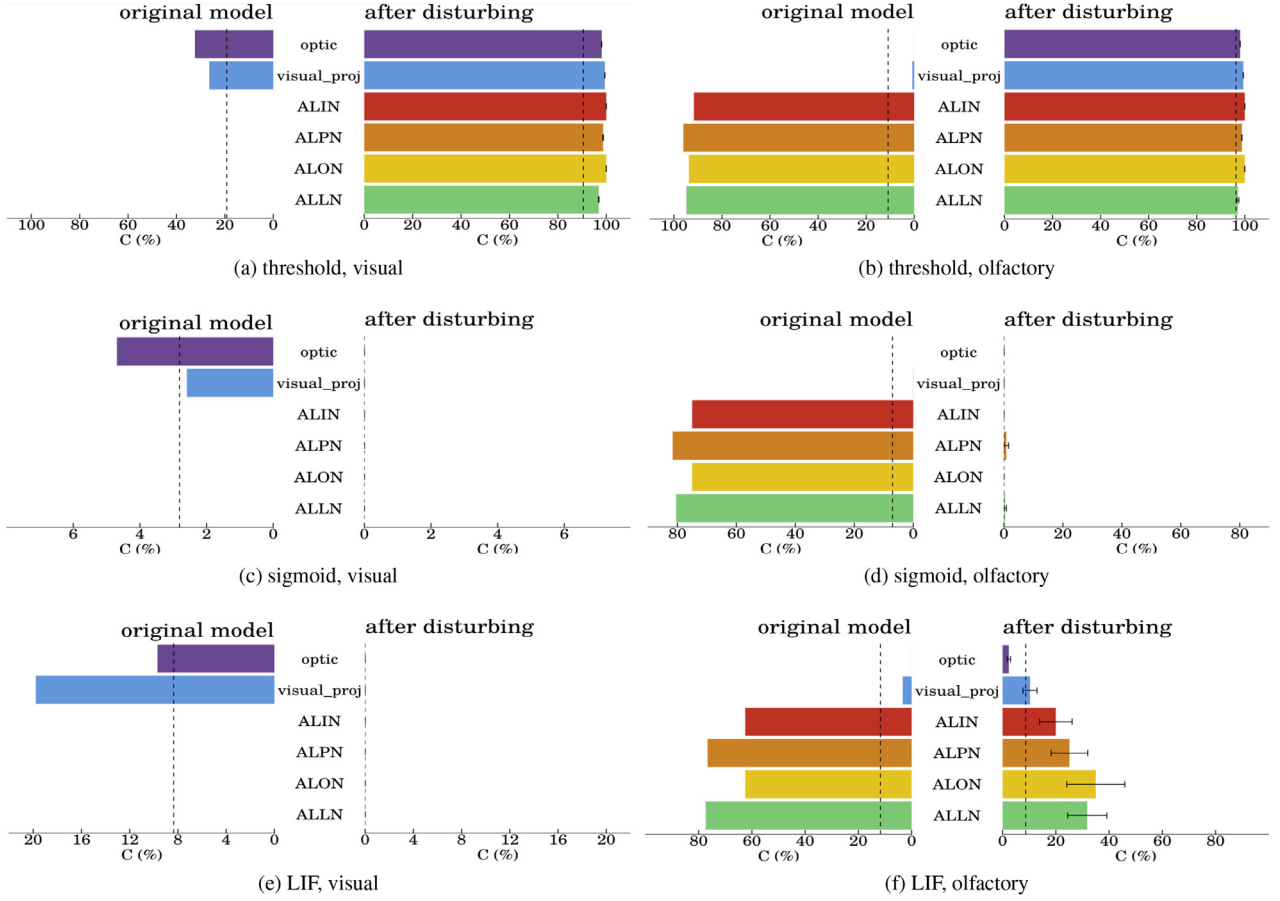
X. Zhang, P. Yang, J. Feng et al.

Fig. 3. Comparative test of intrinsic neurons' activation. For disturbing model, we conduct 5 repeated experiments and take the average and standard deviation. The dotted lines represent average activate rate in brain. In disturbing model, we set reconnect rate $p = 20\%$ and $\sigma = 0.8$.

and olfactory systems and visualized the results as a heat map (Fig. 4(a)). The findings reveal a significant segregation between the visual and olfactory areas. Specifically, within the visual and olfactory areas, there are 13,309,161 and 882,170 synapses, respectively. However, only 1837 synapses exist between these two areas. These interconnecting synapses constitute only approximately 0.0138% and 0.208% of the total synapses within the visual and olfactory areas, respectively.

Fig. 4 (b) represents the schematic diagram of the connection relationships in the neuronal visual and olfactory systems. We use nodes to represent functional areas and use edges to represent synapses between areas. The thickness of edges represents the number of connections. This diagram indicates that the number of connections within regions is significantly greater than the number of inter-regional connections.

These indicate that the network structure between these two functional systems is almost entirely separate.

3.4. Distances between input and activation areas

To further investigate whether this separation phenomenon is caused by greater spatial distance, we calculated the average network distance and spatial distance between different areas of the brain network. The results are presented in Table 3.

The analysis of Table 3 showcases that spatial distances among neurons do not straightforwardly translate to ease of activation. While visual input neurons across all intrinsic areas exhibit similar average spatial distances, quasi-real activation patterns manifest predominantly in specific neural types (optic and visual_projection). Conversely, the average network distances between input neurons and target neurons is notably smaller compared to irrelevant neurons. Specifically, visual input neu-

Table 2
List of Hyperparameters.

Hyperparameter	Description	Value
τ	Membrane Time Constant	15.0 ms
V_{rest}	Resting Membrane Potential	-65 mV
V_{th}	Spike Threshold	-45 mV
R	Membrane Resistance	0.5GΩ
dt	Time Step	0.55 ms
α	Current Proportion Factor	0.03/0.045 (visual/olfactory)

rons exhibit network distances to optic and visual_projection neurons as 5.7018 and 5.7432, respectively, while distances to neurons irrelevant to olfactory (ALLN, ALIN, ALON, and ALPN) are measured at 6.6442, 6.2350, 6.1506, and 6.5380, respectively. This demonstrates that neurons corresponding to visual inputs maintain a generally closer network distance relative to unrelated neurons. Furthermore, neurons associated with olfactory inputs maintain network distances approximately half that of unrelated neurons. These observations suggest that the network distance between input neurons and their specific activation areas is more significant than spatial distance, underscoring the importance of network structure over spatial structure in defining the quasi-real activation patterns of brain networks.

3.5. Bilateral response under unilateral stimulus

In real life, the left and right hemispheres cooperate to perform complex tasks. To examine whether network models can simulate this co-operation, we administered a unilateral stimulus to input neurons and
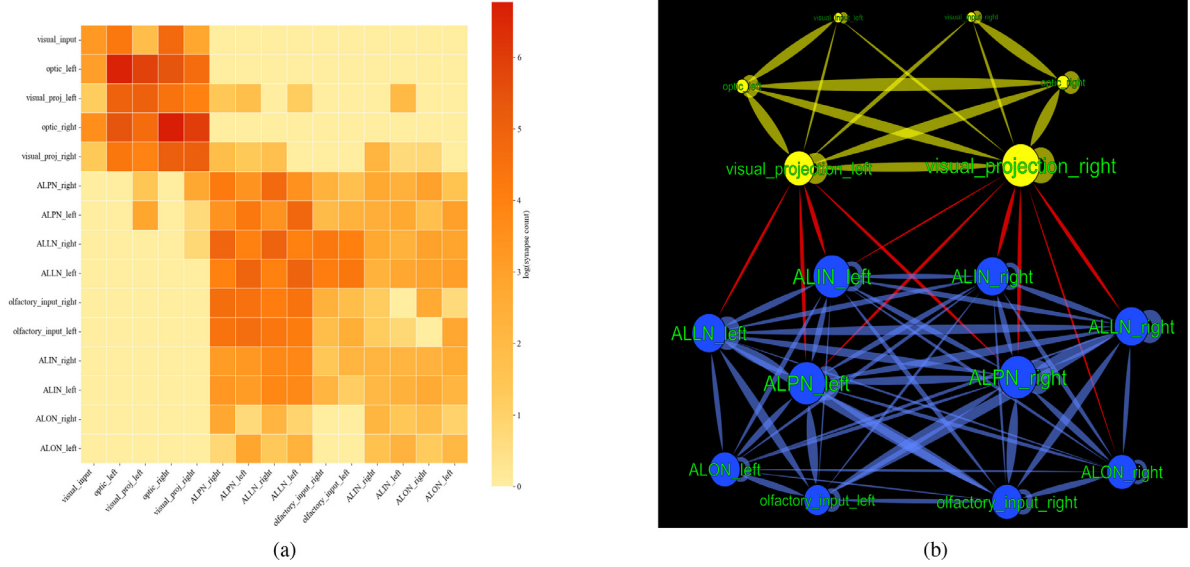
(a)

(b)

Fig. 4. Heatmap and schematic diagram illustrating the connections between areas related to vision and olfaction. (a) presents the heatmap. (b) shows the schematic diagram of the connection relationships.

Table 3

Spatial and network distance between input areas and functional areas.

Input type	Distance type	optic	visual_proj	ALLN	ALON	ALPN	ALIN
Visual input	SpD (nm)	365012	354725	351919	346925	348517	348901
	NeD (edge)	**5.7018**	**5.7432**	6.6442	6.1506	6.5380	6.2350
Olfactory input	SpD (nm)	302690	251144	110827	123179	115089	173345
	NeD (edge)	5.7967	5.1706	**3.4458**	**3.6312**	**3.6820**	**3.3845**

monitored the varying activation ratios across both hemispheres. Specifically, we independently simulated visual input neurons in the left and right hemispheres and recorded the rate of activated neurons in each hemisphere over time. Second, we investigate whether local attack to one side of the network-analogous to real-world conditions such as tumors and other diseases-affects this bilateral response process, and how the extent of such damage influences the synergistic response.

The specific methods of inducing attack are as follows: We first identify two symmetrical coordinates on both hemispheres of the brain. Using these coordinates as the center, we remove nodes within varying radii and subsequently record the response curves for each hemisphere-related region.

Fig. 5 illustrates the specific length measurements of the Drosophila connectome and the regions examined in this study. The purple and blue cells represent neurons associated with visual processing. Spheres S1, S2, S3, and S4 each represent four spherical regions subjected to local-

ized attacks. Sphere S1 and S2 encompass approximately 2000 neurons each, while sphere S3 and S4 each cover approximately 12,000 neurons.

Fig. 6 illustrates the curve depicting how the response ratio evolves with each time step. We use C_{avg} to represent the average activated rate of areas related to vision. Notably, when stimulating one hemisphere alone, visual processing neurons in both hemispheres are activated (see curve regular left and right in Fig. 6(a) and (b)).

Secondly, in the case of different regional node failures, even when roughly 12,000 nodes (approximately 1/10 of the total network nodes and 1/3 of the visually relevant neurons) were deleted, the network ultimately exhibited response characteristics similar to the original curve. This indicates that the network possesses strong robustness facing with local attacks. Additionally, for networks with failures on the input side, a delay in bilateral response curves was observed when the failure radius reached $90\mu m$ ($S4$, left and right stimuli). This suggests that large-scale failures of visually relevant nodes primarily affect the rate at which the
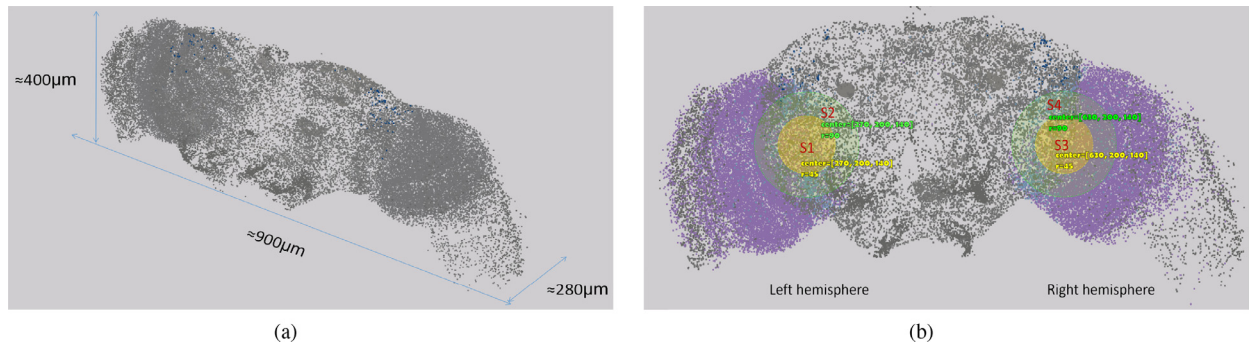

(a)

(b)

Fig. 5. Schematic diagram of the specific length measurements of the Drosophila connectome and the location of regions deleted. (a) illustrates the geometric dimensions of Drosophila connectome. (b) represents the locations of targeted regions. The units of center and r in labels are micrometers.
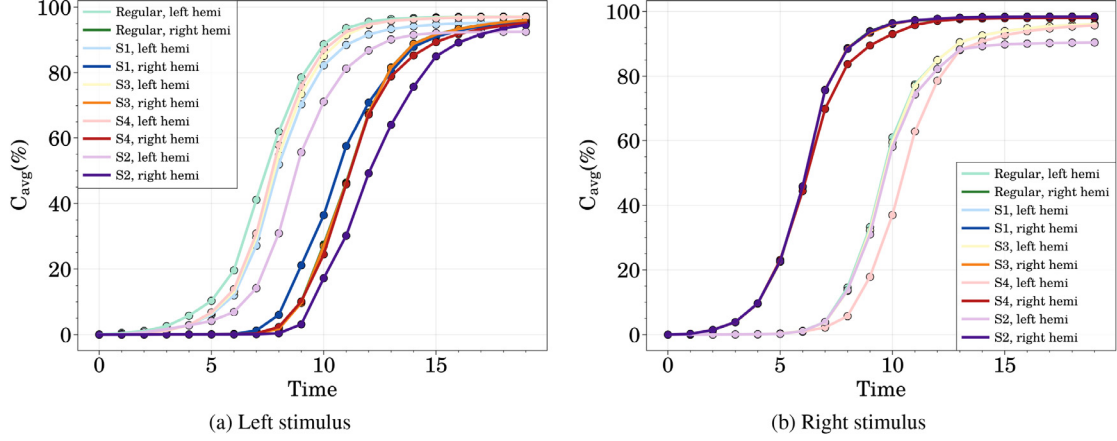
(a) Left stimulus

(b) Right stimulus

Fig. 6. Experiment of activation rate under single stimulus. All responses on the left hemisphere are marked with light-colored lines, and all responses on the right hemisphere are marked with dark-colored lines. We set threshold $\sigma_0 = 0.95$.
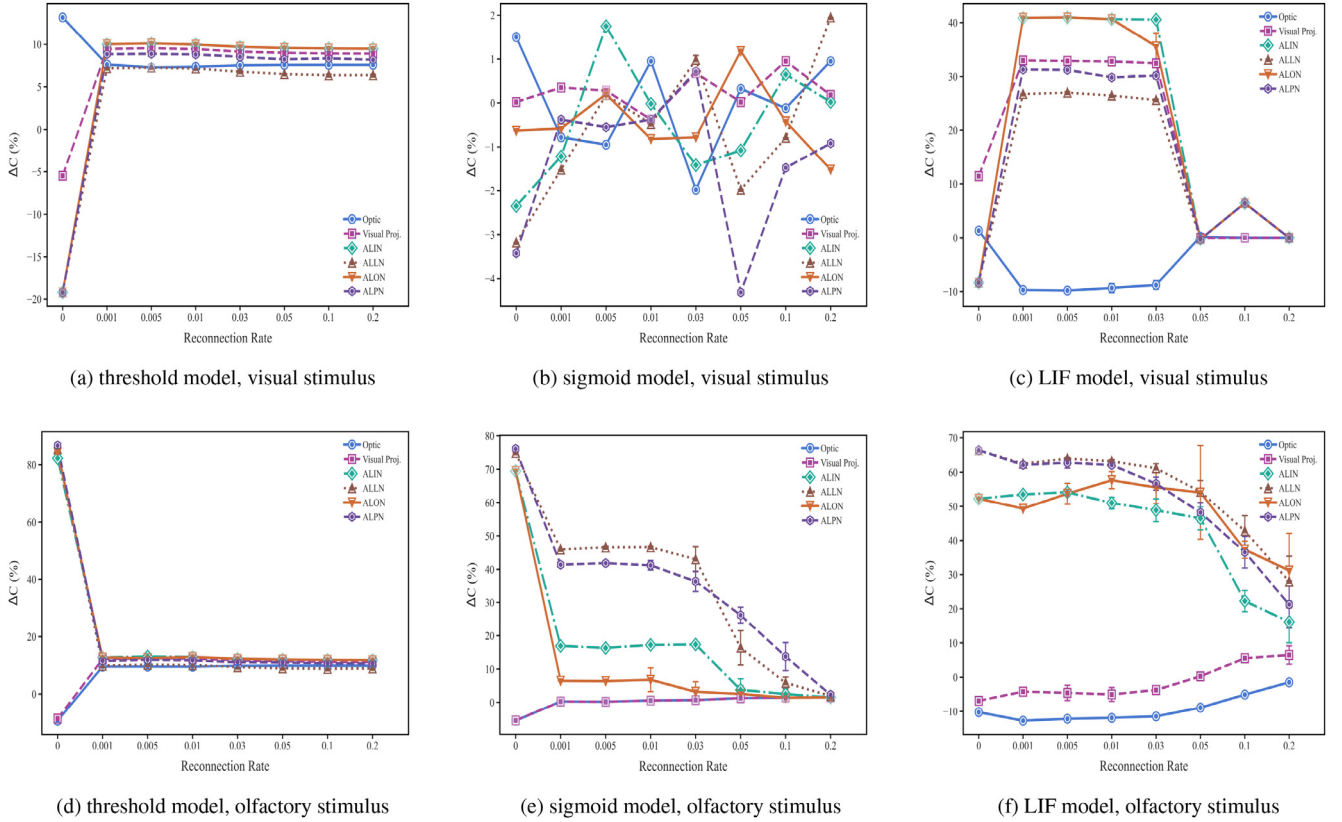

(a) threshold model, visual stimulus

(b) sigmoid model, visual stimulus

(c) LIF model, visual stimulus

(d) threshold model, olfactory stimulus

(e) sigmoid model, olfactory stimulus

(f) LIF model, olfactory stimulus

Fig. 7. Relationships of activation rate with reconnect rate. We conduct 5 repeated experiments and take the average and standard deviation.

visual functional network reaches a steady state, rather than the number of nodes activated at steady state.

Below, we further explain the reasons for the significant delay in responses to unilateral large-scale regional attacks on this side's stimuli (e.g., in Fig. 6a, where the local damaged area is the $S2$ region of the left hemisphere, and stimuli on the left side cause responses in both the left and right hemispheres (light purple and dark purple curves) to be delayed). Calculations show that there are 19,031 synapses from the left hemisphere's visual input area to the left hemisphere's visual signal processing area (optic, visual_projection), while there are only 18 synapses from the left hemisphere's visual input area to the right hemisphere's visual signal processing area. Furthermore, there are 338,456 synapses from the left hemisphere's visual processing area to the right hemisphere's visual signal processing area. This implies that, primarily, the unilateral visual input area essentially does not interact with the con-

tralateral visual signal processing area, and interactions occur indirectly through the ipsilateral visual processing area. Consequently, when the visual signal processing area of this side is damaged, the reduction in the number of neurons makes it challenging for the remaining neurons to reach an excitatory state, causing delays in the ipsilateral visual signal processing area. This delay, in turn, leads to delayed responses in the contralateral visual signal processing area.

3.6. Impact of perturbation rate on activation areas

In this section, we discuss the impact of different reconnection rates on activation patterns using the degree-preserving reconnection method.

The experiments presented in this section involve calculating patterns induced by two types of stimuli across three models under net-

work perturbations of 1%, 5%, 1%, 3%, 5%, 10%, and 20% reconnect rates. The reconnect rate p in degree-preserving rewiring refers to the proportion of edges that are randomly rewired while maintaining the degree (number of connections) of each node unchanged. Let C be the average activation ratio of an area. We normalized each data point using the difference between the activation ratio of this area and the average activation ratio $\bar{C}$ of the entire brain, that is to say, $\Delta C = C - \bar{C}$.

The experimental results are shown in Fig. 7, where 0 represents the original, unperturbed experimental results. At the 0 point, there is a significant difference in the relative activation ratios between visual and olfactory areas under specific stimuli. However, this significant activation pattern, discussed in the main text, disappears with a 1%'s network perturbation, replaced by a roughly equal activation ratio across all regions. This indicates that even a 1%'s change in network structure can lead to a rapid loss of network functionality specificity. Additionally, small-scale network perturbations (1%-5%) have a lesser impact on olfactory stimuli compared to visual stimuli. This is because the number of neurons associated with olfactory functions is significantly fewer than those related to visual functions, making it less likely for small-scale network structure changes to affect these neurons, thereby leading to a smaller impact on functionality.

Horizontal comparisons indicate that while there are no significant differences among different models in forming activation patterns, more complex neuron models better maintain their original activation patterns under network disturbances. This is because signals generated by complex neuron models have greater redundancy and functional diversity. For instance, the LIF (Leaky Integrate-and-Fire) model has a voltage decay mechanism, where the voltage gradually decays in the absence of a signal. Even if some input signals are erroneous, as long as the proportion of errors is not very large, the decay mechanism can filter out the impact of these erroneous signals.

4. Conclusion and discussion

Our study, which utilized a large-scale network communication model derived from the Drosophila connectome, highlights the crucial importance of neural network architecture in generating brain-like activation patterns.

We first analyzed the structure of the Drosophila brain network, including the basic statistical properties and the symmetry of the network. An interesting phenomenon observed is the correlation between neuronal degree and geometric size: Fig. 2e demonstrates that the number of synapses formed by a neuron (represented by degree) increases logarithmically, rather than linearly, with respect to its surface area, volume, or length. These characteristics of the brain can be explained by the Weber-Fechner's law: for any sensory pattern, the perceived intensity is a logarithmic function of the physical intensity. Specifically, the size, length, and area changes can only cause a logarithmic change in the number of synapses the neuron has. These results suggest that although synaptic plasticity lead to a continuous increase in the number of synapses between neurons and other cells, this logarithmic relationship makes it difficult for the number of synapses formed by a neuron to increase indefinitely. This may account for the overall power-law distribution observed in Fig. 2e.

To examine the impact of neuronal activation mechanisms on the generation of realistic network patterns, we simulated three activation mechanisms for specific inputs. From the most conventional threshold models to more refined ones, it can be observed that the granularity of the model has minimal impact on the formation of these quasi-real activation patterns. This suggests that, relative to the precision of the activation mechanism, the unique structural properties exert a more significant influence on the emergence of such quasi-realistic activation patterns. The brain's unique network structure plays a crucial role in this realistic activation mechanism, aligning with studies on complex systems where the organization and interaction structure among individu-

als, rather than individual capabilities, determine emergent phenomena [24].

To elucidate the influence of network structure on function, we analyzed the topology of the network (Fig. 4 and Table 3). These results collectively suggest that network architecture, rather than spatial structure or activation mechanisms, is the primary determinant of the Drosophila connectome's ability to generate quasi-real activation patterns, owing to its unique connectivity profile.

To test the impact of network perturbation ratio on its functionality, we calculated activation patterns with different reconnect rates (Fig. 7). These results indicate that the formation of realistic activation patterns is highly sensitive to changes in network structure, with even minor perturbations capable of disrupting this network configuration. This indirectly substantiates that the authentic network structure is crucial for the formation of genuine activation patterns. Additionally, it highlights that complex functions (such as vision) are more susceptible to network disturbances. Conversely, Fig. 6 shows that the network retains its original performance under a region-based attack. One explanation for these findings is that random rewiring thoroughly alters the network topology, potentially disrupting original functional modules and pathways, which leads to disordered information transmission paths and significantly impacts activation patterns. Additionally, because rewiring is global and random, it induces unpredictable perturbations that undermine redundancy and fault tolerance mechanisms, rendering the network more sensitive to such global disturbances. In contrast, the reason the network's dynamic properties remain relatively stable after the deletion of nodes within a specific region is that this perturbation is localized and has a minor impact on the global topology. Moreover, random rewiring may affect critical nodes or key pathways within the network, leading to significant functional impairment of the overall network. However, regional node deletion, if involving non-critical nodes and edges, may not significantly impact the network's functionality, allowing it to maintain normal activation patterns.

To evaluate the impact of the observed network structural symmetry (Fig. 2b, c, and d), we input visual signals separately to the left and right hemispheres and observed the effects. The findings in Fig. 6 reflect real-world phenomena: Although the left and right hemispheres possess certain functional specializations, they also exhibit synergistic effects and typically collaborate to fulfill specific functions [25]. For example, during complex cognitive tasks, both hemispheres coordinate their efforts to achieve task completion. The experimental results indicate that similar synergistic effects emerge even when only the neurons on one side of the brain are stimulated, indirectly validating the model's effectiveness. Moreover, the network maintains similar synergistic effects even in the face of large-scale localized attacks, indirectly demonstrating the network's robust resilience. Finally, by analyzing the connections between different regions, it is found that the cause of these synergistic effects is not the connections between visual input and contralateral visual processing areas, but rather the extensive connections within the visual processing regions themselves. This provides a new perspective for understanding the brain's synergistic effects.

These findings have profound implications for advancing the study of both biological and artificial intelligence. In biological intelligence, it is demonstrated that the brain's network architecture-rooted in the complexity of individual neurons-plays a dominant role in generating intelligence-related activation patterns. This challenges the traditional neuroscience focus on the dynamics of individual neurons by emphasizing the importance of the brain's global network structure. For artificial intelligence research, the results suggest that current AI architectures might benefit from redesigning to more effectively mimic the structural characteristics of biological neural networks. From a complexity science perspective, these findings reveal how global intelligent behavior can emerge from simple local interaction rules, illustrate the critical balance between modularity and integration in determining system efficiency, and highlight how network structure influences resilience to failures. Specifically, a number of technological innovations in the de-

sign of neural networks that emulate biological systems may be fostered, such as decentralized AI systems, brain-inspired network design, and interhemispheric communication models. These insights not only provide direction for developing more brain-like artificial intelligence but also offer new frameworks for understanding and designing various complex intelligent systems, with significant implications for both technological innovation and organizational design.

Data and code availability

The dataset of Drosophila brain connectome is from [14,15]. All codes necessitate the reproduction of the results in this paper is available at https://github.com/XiaoyuZhang001/Drosophila.

Declaration of competing interest

The authors declare that they have no conflicts of interest in this work.

Acknowledgments

Supplementary material

Supplementary material associated with this article can be found, in the online version, at 10.1016/j.fmre.2025.01.017

References

[1] T.N. Lerner, L. Ye, K. Deisseroth, Communication in neural circuits: tools, opportunities, and challenges, Cell 164 (6) (2016) 1136–1150.

[2] A. Zador, S. Escola, B. Richards, et al., Catalyzing next-generation artificial intelligence through neuroai, Nat. Commun. 14 (1) (2023) 1597.

[3] A. Avena-Koenigsberger, B. Misic, O. Sporns, Communication dynamics in complex brain networks, Nat. Rev. Neurosci. 19 (1) (2018) 17–33.

[4] P. Lansky, S. Ditlevsen, A review of the methods for signal estimation in stochastic diffusion leaky integrate-and-fire neuronal models, Biol. Cybern. 99 (4) (2008) 253–262.

[5] A.L. Hodgkin, A.F. Huxley, A quantitative description of membrane current and its application to conduction and excitation in nerve, J. Physiol. (Lond.) 117 (4) (1952) 500.

[6] H.C. Tuckwell, Introduction to Theoretical Neurobiology: Linear Cable Theory and Dendritic Structure, vol. 1, Cambridge University Press, 1988.

[7] Y. Zeng, D. Zhao, F. Zhao, et al., Braincog: a spiking neural network based, brain-inspired cognitive intelligence engine for brain-inspired ai and brain simulation, Patterns 4 (8) (2023) 100789.

[8] C. Seguin, O. Sporns, A. Zalesky, Brain network communication: Concepts, models and applications, Nat. Rev. Neurosci. 24 (9) (2023) 557–574.

[9] J.G. Greener, S.M. Kandathil, L. Moffat, et al., A guide to machine learning for biologists, Nat. Rev. Mol. Cell Biol. 23 (1) (2022) 40–55.

[10] X. Zhang, W. Yang, J. Feng, et al., Gspect: spectral filtering for cross-scale graph classification, IEEE Trans. Network Sci. Eng. 12 (1) (2025) 547–558, doi:10.1109/TNSE.2024.3513456.

[11] J. Kaplan, S. McCandlish, T. Henighan, et al., Scaling laws for neural language models, arXiv preprint arXiv:2001.08361 (2020).

[12] N.K. Logothetis, What we can do and what we cannot do with fMRI, Nature 453 (7197) (2008) 869–878.

[13] M. Winding, B.D. Pedigo, C.L. Barnes, et al., The connectome of an insect brain, Science 379 (6636) (2023) eadd9330.

[14] S. Dorkenwald, A Matsliah, A.R. Sterling, et al., Neuronal wiring diagram of an adult brain, Nature 634 (8032) (2024) 124–138.

[15] P. Schlegel, Y. Yin, A.S. Bates, et al., Whole-brain annotation and multi-connectome cell typing of Drosophila[J], Nature 634 (8032) (2024) 139–152.

[16] M. Fauth, F. Wörgötter, C. Tetzlaff, The formation of multi-synaptic connections by the interaction of synaptic and structural plasticity and their functional consequences, PLoS Comput. Biol. 11 (1) (2015) e1004031.

[17] M. Pósfai, B. Szegedy, I. Bačić, et al., Impact of physicality on network structure, Nat. Phys. 20 (2024) 142–149.

[18] A. Lin, R. Yang, S. Dorkenwald, et al., Network statistics of the whole-brain connectome of Drosophila[J], Nature 634 (8032) (2024) 153–165.

[19] M. Kaiser, M. Goerner, C.C. Hilgetag, Criticality of spreading dynamics in hierarchical cluster networks without inhibition, New J. Phys. 9 (5) (2007) 110.

[20] C. Seguin, M. Jedynak, O. David, et al., Communication dynamics in the human connectome shape the cortex-wide propagation of direct electrical stimulation, Neuron 111 (9) (2023) 1391–1401.

[21] M. Suzuki, C.M. Pennartz, J. Aru, How deep is the brain? The shallow brain hypothesis, Nat. Rev. Neurosci. 24 (12) (2023) 778–791.

[22] S. Peron, F. Gabbiani, Spike frequency adaptation mediates looming stimulus selectivity in a collision-detecting neuron, Nat. Neurosci. 12 (3) (2009) 318–326.

[23] D.R. Chialvo, Critical brain networks, Physica A 340 (4) (2004) 756–765.

[24] J.H. Holland, Emergence: From Chaos to Order, OUP Oxford, 2000.

[25] L.W. Swanson, Brain Architecture: Understanding the Basic Plan, Oxford University Press, USA, 2012.

Author profile

Xiaoyu Zhang received the BE degree in automation from the National University of Defense Technology, Changsha, China. He is currently a PhD student at the College of Systems Engineering, National University of Defense Technology. His research interests include complex systems, physical networks and artificial intelligence.

Xin Lu obtained his PhD from Department of Public Health Sciences at Karolinska Institutet, Stockholm, Sweden. He is the co-founder of Flowminder Foundation, and professor at the National University of Defense Technology in China. His research interests include big data analytics, complex networks, human behavior and emergency management.